Electronic Supplementary Material (ESI) for Reaction Chemistry & Engineering.

Supporting Information

Understanding the impact of small vanadia clusters and their coverage effects on undoped and Ni-doped ceria nanorod supports on propane oxidative dehydrogenation

*Anoop P Pushkar, Jithin John Varghese**

Department of Chemical Engineering, Indian Institute of Technology Madras, Chennai 600036, India

*Corresponding Author: **E-mail**: jithinjv@iitm.ac.in; **Phone**: +91-44-22574182

Table S1. Test details for analyzing the impact of adding Hubbard U corrections for Ni dopant.

Interaction type	**E_{ads} / E_a Without U on Ni 3d**	**E_{ads} / E_a With U on Ni 3d (U_{eff} = 5.3)**[1,2]
H adsorption over site S1	-1.40 eV	-1.36 eV
H adsorption over S4	-1.66 eV	-1.65 eV
Propane first C-H activation over S1	1.36 eV	1.31 eV
Propane first C-H activation over S4	0.90 eV	0.93 eV

The inclusion of U correction for Ni led to energy variations of 0.01-0.04 eV for H adsorption steps and 0.03-0.05 eV for C-H activation steps (E_a). Such variations in energies do not significantly impact the qualitative trends in the energetics reported in this study. This observation was mainly due to Ni not interacting directly with any of the reactant atoms such as H or C, as its interaction is strongest with that of VO_2 and surrounding surface oxygens. Moreover, the impact of inclusion of U correction for Ni was very small only on local surface oxygens that interact with Ni (S1, S2, bridged oxygen) and was almost negligible on the surface oxygens far from Ni (such as S3, S4 and others).

It should be noted that the impact of U corrections can be different for different catalytic systems depending upon the kind of interactions between the Ni dopant and the host metal oxides. Moreover, the impact will also vary according to the U value chosen, however there are no clear protocols to choose U value for dopants and a conventional choice is that of bulk oxide of the dopant.

Table S2. Test details for choosing electronic convergence criteria for the calculations.

Interaction type	**System**	**E_{ads} / E_a for Electronic convergence: 10^{-4} eV**	**E_{ads} / E_a for Electronic convergence: 10^{-5} eV**
H adsorption	$VO_2/CeO_2(110)$	-1.32 eV	-1.34 eV
H adsorption	$VO_2/Ce_{0.83}Ni_{0.17}O_2$ (110)	-1.40 eV	-1.42 eV
Propane first C-H activation	$VO_2/CeO_2(110)$	1.49 eV	1.53 eV

On analysis of the adsorption and activation energies in Table 1, it was inferred that the electronic convergence of 10^{-4} eV gave sufficient accuracy for this study. A tighter convergence criterion which comes at a higher computational cost would change the energies by only 0.02-0.04 eV for H adsorption and propane C-H activation and would not significantly influence the qualitative trends in the energetics that are reported in this work.

Table S3. Test details for identifying the optimum Ni doping position in the $VO_2/Ce_{0.89}Ni_{0.11}O_2(111)$ catalyst model based on the Vanadia monomer (VO_2) formation energies over different doped structures.

$VO_2/Ce_{0.89}Ni_{0.11}O_2$ (111)	
Ni site Type	**VO_2 formation energy (eV)**
S1	-10.36
S2	-10.29
S3	-9.07
S4	-9.40

Here, S1-S4 were the different surface-doped configurations obtained by replacing one of the surface Ce atoms in the CeO_2 (110) catalyst model with a Ni atom.. The formation energy was calculated according to the reaction,

$$V_{(s)} + Ce_{0.83}Ni_{0.17}O_{2\,(surf)} + O_{2\,(g)} \rightarrow VO_2/Ce_{0.83}Ni_{0.17}O_{2\,(surf)}$$

S1 configuration was found to be the most favorable for VO_2 formation and hence the corresponding Ni dopant position was deemed optimal for our model used in this work. The above test configurations are shown in Figure S1.

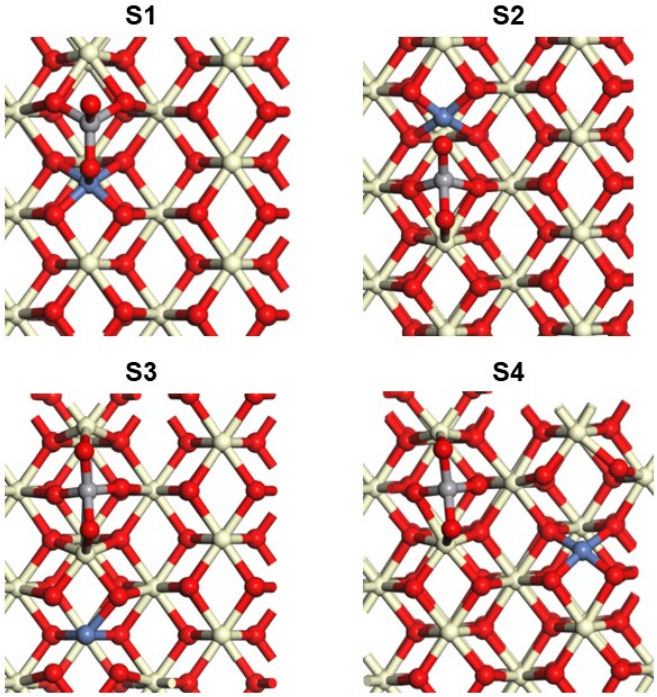

Figure S1. Test configurations used for allocation of optimal Ni dopant position in $VO_2/Ce_{0.83}Ni_{0.17}O_2$ (110) catalysts. The color convention is the same as that mentioned in Figure 1 of the main manuscript.

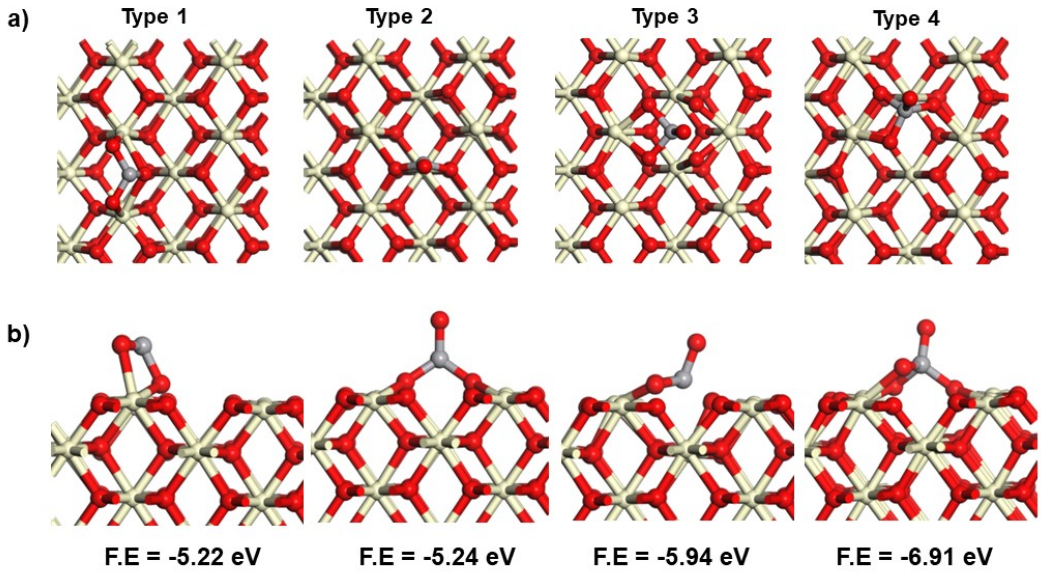

Figure S2. a) Top and b) Front views of test configurations used for obtaining the optimal VO adsorbate configuration over VO/CeO_2 (110) surface that is used for the surface phase equilibria analyses discussed in Section 3.1 of the main manuscript. The color convention of the atoms is the same as in Figure 1 of the main manuscript. The formation energy was calculated according to the reaction,

$$V_{(s)} + CeO_{2\,(surf)} + \frac{1}{2}O_{2\,(g)} \rightarrow VO/CeO_{2\,(surf)}$$

Type 4 was considered as the optimal configuration for further studies as it formed more favorably. A configuration similar to Type 4 was considered for modeling $VO/Ce_{0.83}Ni_{0.17}O_2$ (110) system as well.

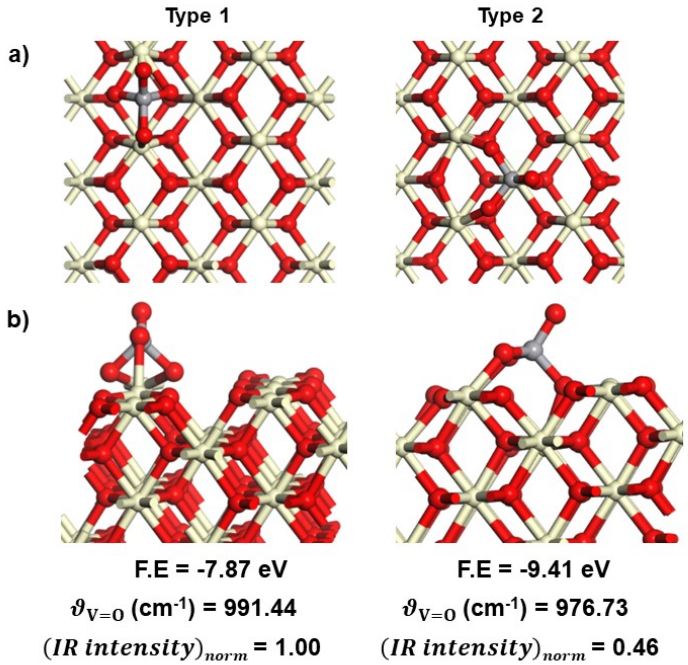

Figure S3. a) Top and b) Front views of Test configurations used for obtaining the optimal VO_2 adsorbate configuration over VO_2/CeO_2 (110) surface that is used for the surface phase equilibria analyses discussed in Section 3.1 of the main manuscript. The color convention is the same as in Figure 1 of the main manuscript. The formation energy was calculated according to the reaction,

$$V_{(s)} + CeO_{2\,(surf)} + O_{2\,(g)} \rightarrow VO_2/CeO_{2\,(surf)}$$

Although Type 2 had more favorable formation energy, the characteristic V=O stretching frequency calculated (976.73 cm^{-1}) using computational IR analyses was in less agreement with the reported experimental V=O IR stretching frequency (1003 cm^{-1})[3], compared to that of Type 1 configuration (991.44 cm^{-1}). Further, the V=O stretch was also less intense in the Type 2 configuration compared to that the in Type 1 configuration. Hence Type 1 was considered the optimal configuration for further studies. Moreover, the H adsorption energies tabulated in Table S2 showed that the oxygens of Type 2 configurations were also less active than those of Type 1. A configuration similar to Type 1 was considered for modeling $VO_2/Ce_{0.83}Ni_{0.17}O_2$ (110) system as well.

Table S4. H adsorption energies over different configurations of VO_2 in VO_2/CeO_2 (111) surface

O-type	H adsorption energies over VO_2/CeO_2 (110) (eV)	
	Type 1	Type 2
bridged	-1.02	-0.72
vanadyl	-0.97	-0.79

Here, the oxygens of Type 2 configuration of VO_2 were deemed less active than that of Type 1 configuration as the H adsorption energies were less negative over Type 2 compared to that over Type 1. Hence, Type 2 configuration could potentially be an inactive VO_2 species compared to Type 1 and may not impact the surface reactivity significantly.

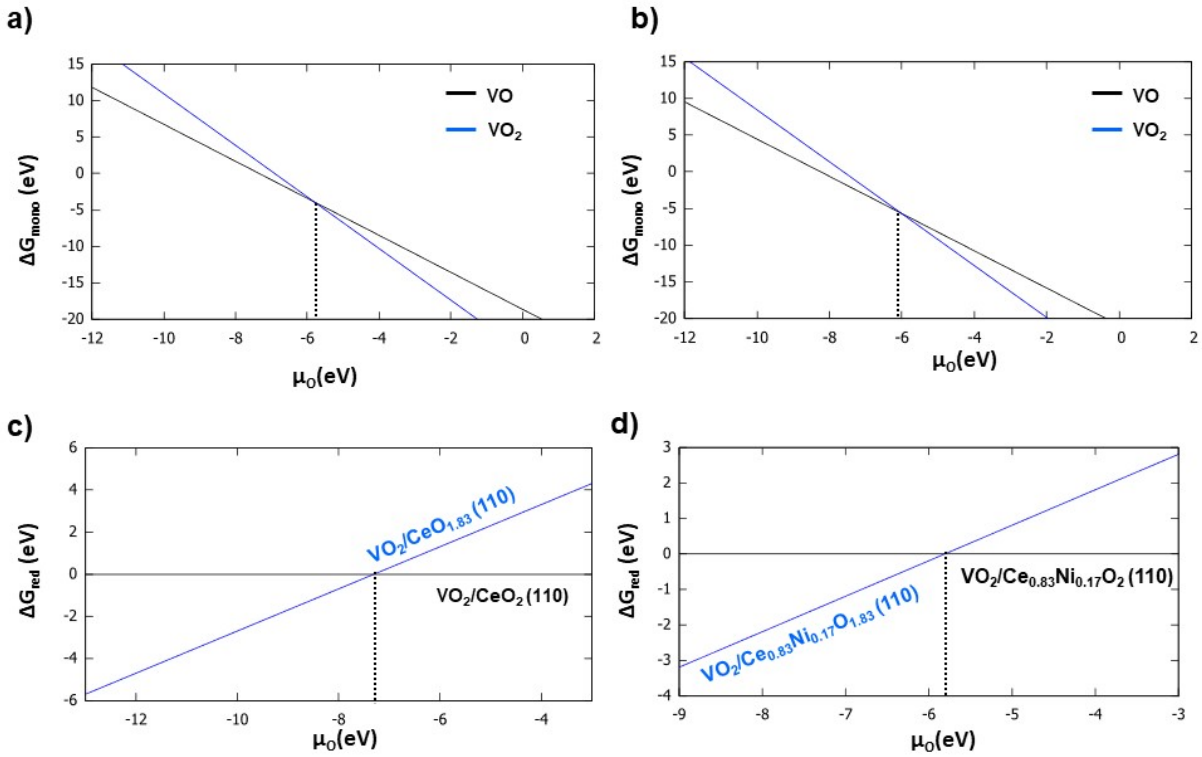

Figure S4: Gibbs free energy change as a function of gas-phase oxygen chemical potential for a), b) vanadia monomer formation and c), d) surface reduction over Ceria and Ni doped ceria nanorod supported Vanadia catalysts respectively. The dashed lines indicate the chemical potentials required for phase transitions.

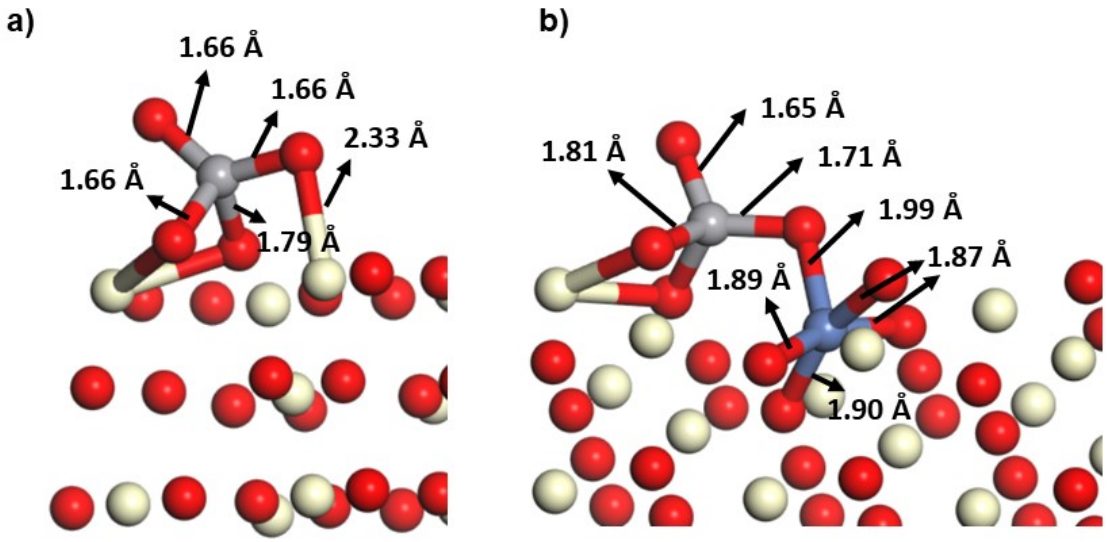

Figure S5. Vanadia to surface oxygen coordination and the corresponding bond lengths in a) $VO_2/CeO_2(110)$ and b) $VO_2/Ce_{0.83}Ni_{0.17}O_2(110)$ surfaces. Here, the VO_2 monomer was stabilized more by $Ce_{0.83}Ni_{0.17}O_2(110)$ than the CeO_2 (110) as the bridged oxygen to Ni bond length (1.99 Å) was lower compared to the bridged oxygen to Ce (2.33 Å). For color conventions of atoms, please refer to Figure 1 of the main manuscript.

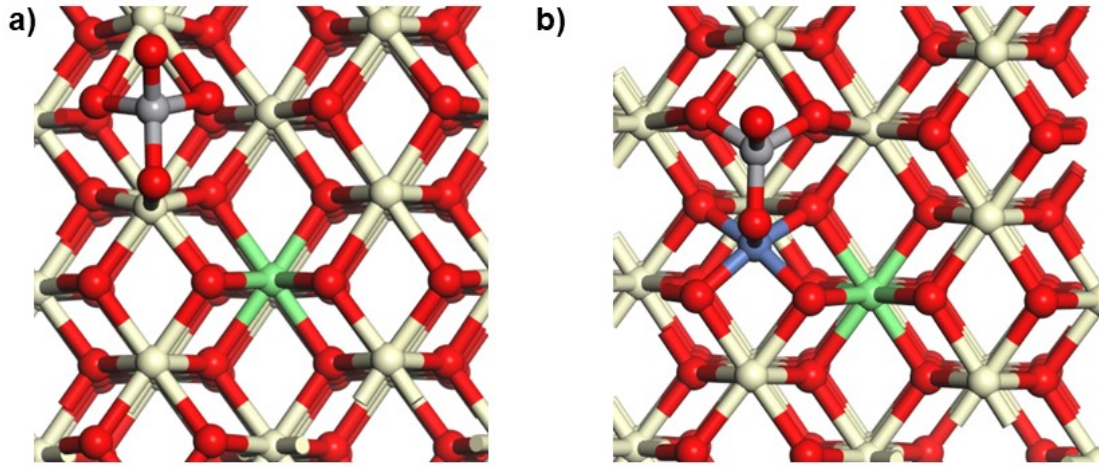

Figure S6. Sub-surface Ce reduction due to electron transfer from V to CeO_2 surface in a) $VO_2/CeO_2(110)$ and b) $VO_2/Ce_{0.83}Ni_{0.17}O_2(110)$ surfaces. Here, the Ce^{+3} is denoted in green colour, while the color conventions of other atoms are same as that mentioned in Figure 1 of the main manuscript. The Bader charges of the highlighted Ce in $VO_2/CeO_2(110)$ and $VO_2/Ce_{0.83}Ni_{0.17}O_2(110)$ surfaces were found to be +1.94 and +1.96*e* respectively, which were closer to that of Ce^{+3} in bulk Ce_2O_3 (+1.95*e*).

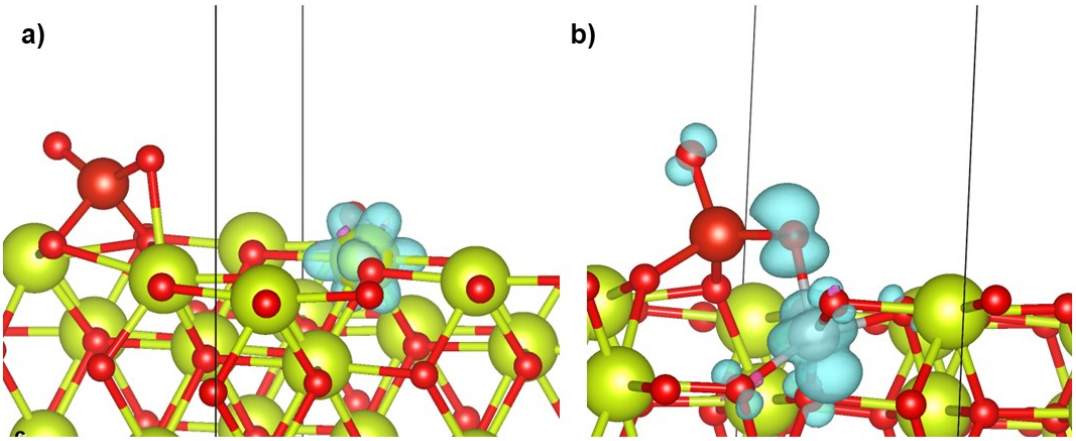

Figure S7. Spin density analyses showing excess electron (blue-colored) clouds over a) VO_2/CeO_2 (110); b) $VO_2/Ce_{0.83}Ni_{0.17}O_2$ (110) surfaces. The presence of excess electron clouds is the outcome of electron donation by V of VO_2 to CeO_2 (110) and $Ce_{0.83}Ni_{0.17}O_2$ (110) surfaces. The localization of excess electron clouds over vanadyl and bridged oxygens of $VO_2/Ce_{0.83}Ni_{0.17}O_2$ (110) surface indicates enhancement in their potencies, which is in line with the observations made by H adsorption and Bader charge analyses (refer to Section 3.2 of the main manuscript).

Table S5. Impact of inclusion of Van der Waals force corrections on the formation energies of different states in the S1-O_{bridge} pathway (please refer to Figure 3 of the manuscript) over VO_2/CeO_2 (110) catalyst, calculated using the bare catalyst and propane as the references (F.E = E_{int} - E_{cat} -$E_{propane}$)

Elementary steps	F.E computed with Van der Waals Force corrections (Grimme's DFT-D3 method) (eV)	F.E computed without Van der Waals Force corrections (eV)
Physisorbed C_3H_8	-0.49	-0.07
TS1	1.00	1.66
Physisorbed $C_3H_7^{\bullet}$	0.48	0.79
Physisorbed C_3H_6	-1.55	-0.73

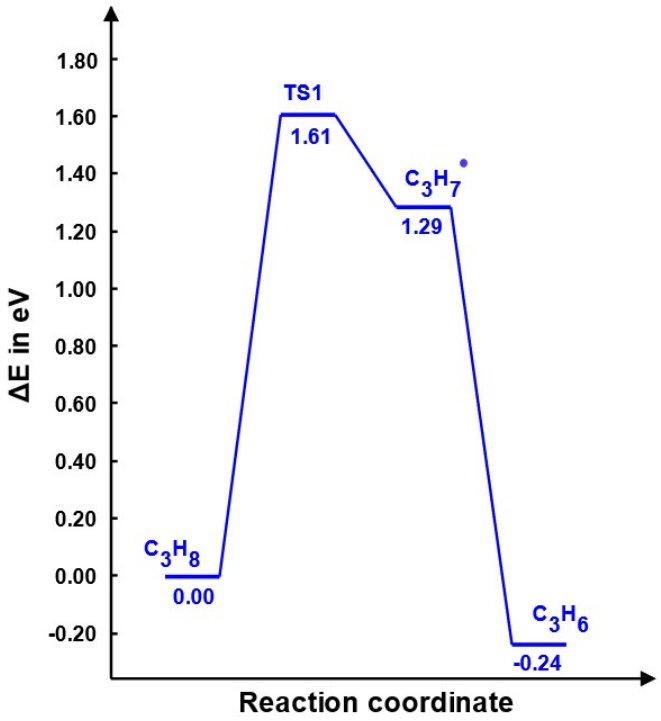

Figure S8. Energy profile for propane ODH (isopropyl mediated) over $VO_2/CeO_2(110)$ surface initiated by vanadyl oxygen. This denotes $O_{vanadyl}$- O_{bridge} path, where the second C-H activation occurred spontaneously over the bridged oxygen. The propane C-H activation required very high energy barrier (1.61 eV) over the vanadyl oxygen and was in line with the less favorable H adsorption energy predicted in Table 1 of the main manuscript.

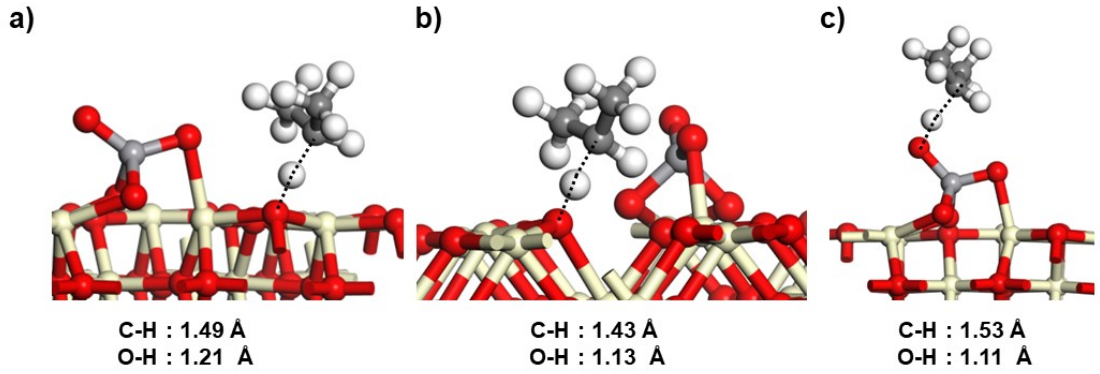

Figure S9. Structures and the activated bond lengths of the transition states in propane ODH mechanisms (isopropyl radical mediated) over $VO_2/CeO_2(110)$ surface, as shown in a) S1-O_{bridge} path, b) S4-O_{bridge} path of Figure 3 of the main manuscript, and c) $O_{vanadyl}$-O_{bridge} path in Figure S7. Here, the cream, red, light grey, white and dark grey atoms denote Ce, O, V, H and C atoms, respectively.

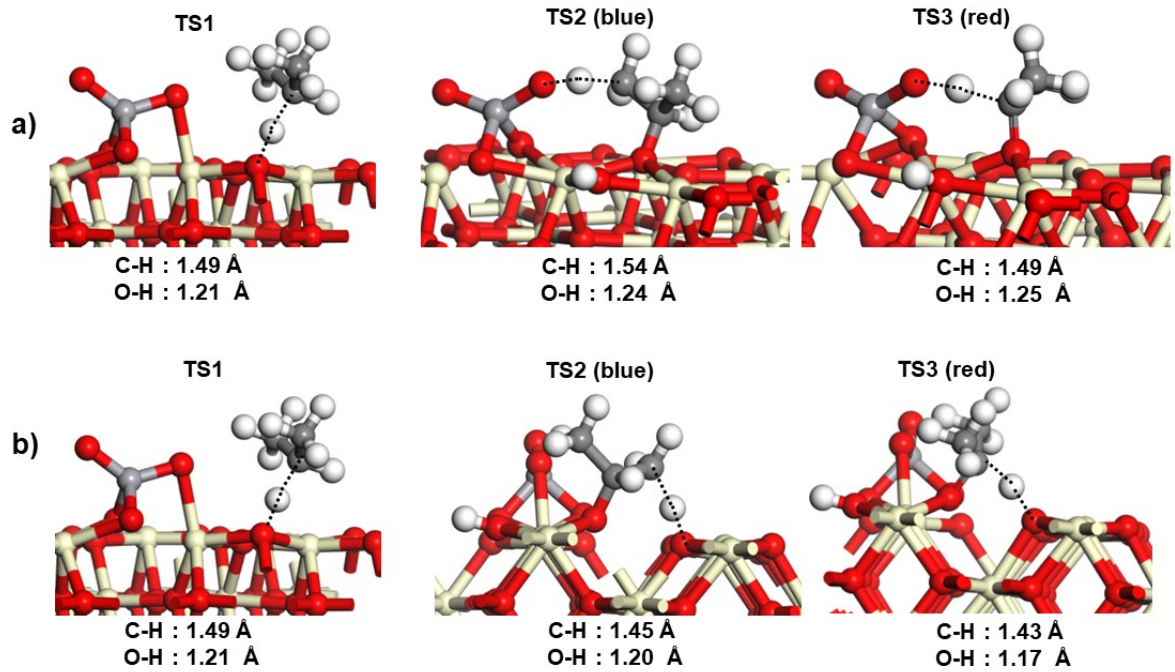

Figure S10. Structures and the activated bond lengths of the transition states in propane ODH mechanisms (isopropoxide mediated) over $VO_2/CeO_2(110)$ surface, as shown in a) S1-S2-O_{bridge} path, b) S1-S2-S3 path of Figure 4 of the manuscript. Here, the cream, red, light grey, white and dark grey atoms denote Ce, O, V, H and C atoms, respectively.

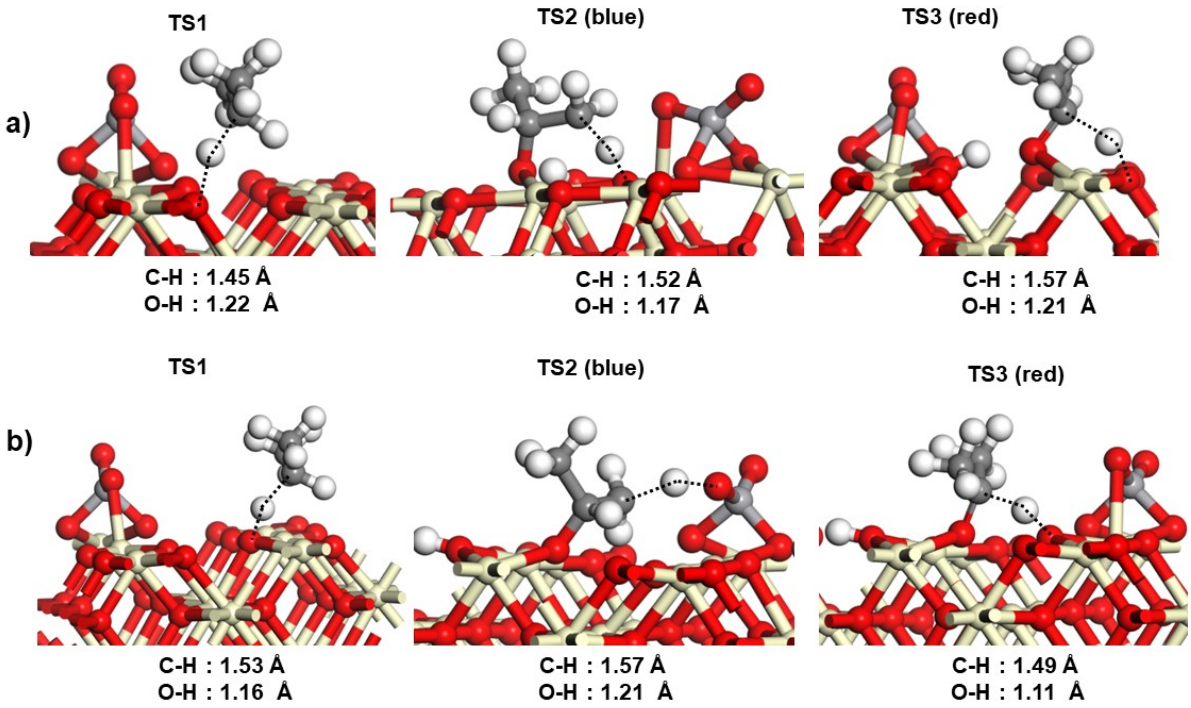

Figure S11. Structures and the activated bond lengths of the transition states in propane ODH mechanisms (isopropoxide mediated) over $VO_2/CeO_2(110)$ surface, as shown in a) S2-S3-S7/S4 path, b) S3-S4-O_{bridge}/S1 path of Figure 5 of the manuscript. Here, the cream, red, light grey, white and dark grey atoms denote Ce, O, V, H and C atoms, respectively.

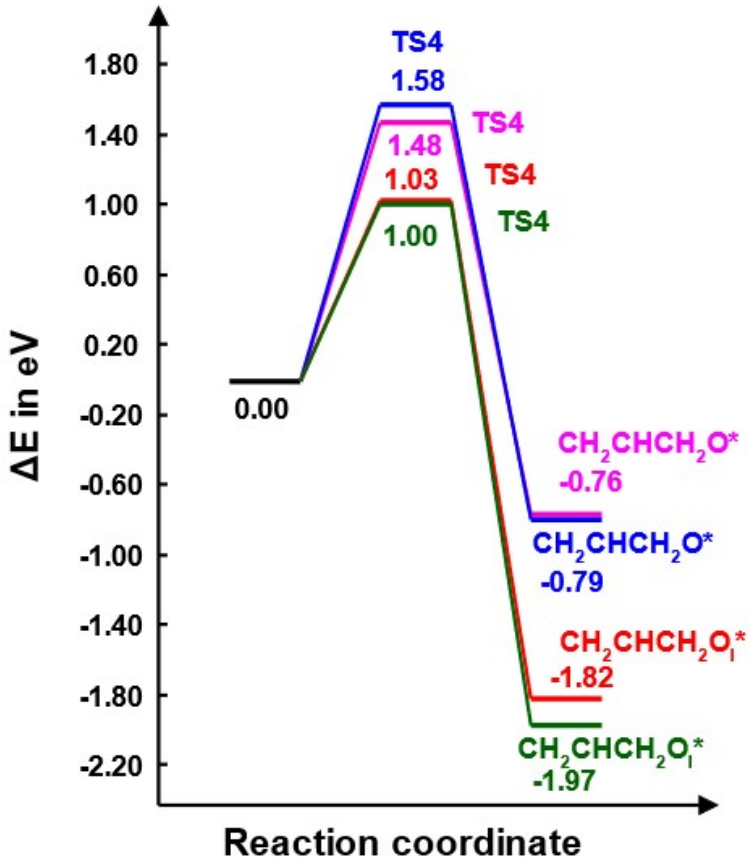

Figure S12. Energy profiles for propene C-H activation steps, denoting the onset of sequential oxidation route for propane oxidation via propene formation over $VO_2/CeO_2(110)$ surface. Here blue, purple, red, and green paths denote propene activation over vanadyl, bridged, site S2, and site S3 surface oxygens respectively. The vanadyl and bridged oxygens offered low kinetic favorability, while the surface oxygens - sites S2, and S3 were the most favorable sites for propene activation. (Refer to Figure 1 of the main manuscript for the oxygen site numbering convention)

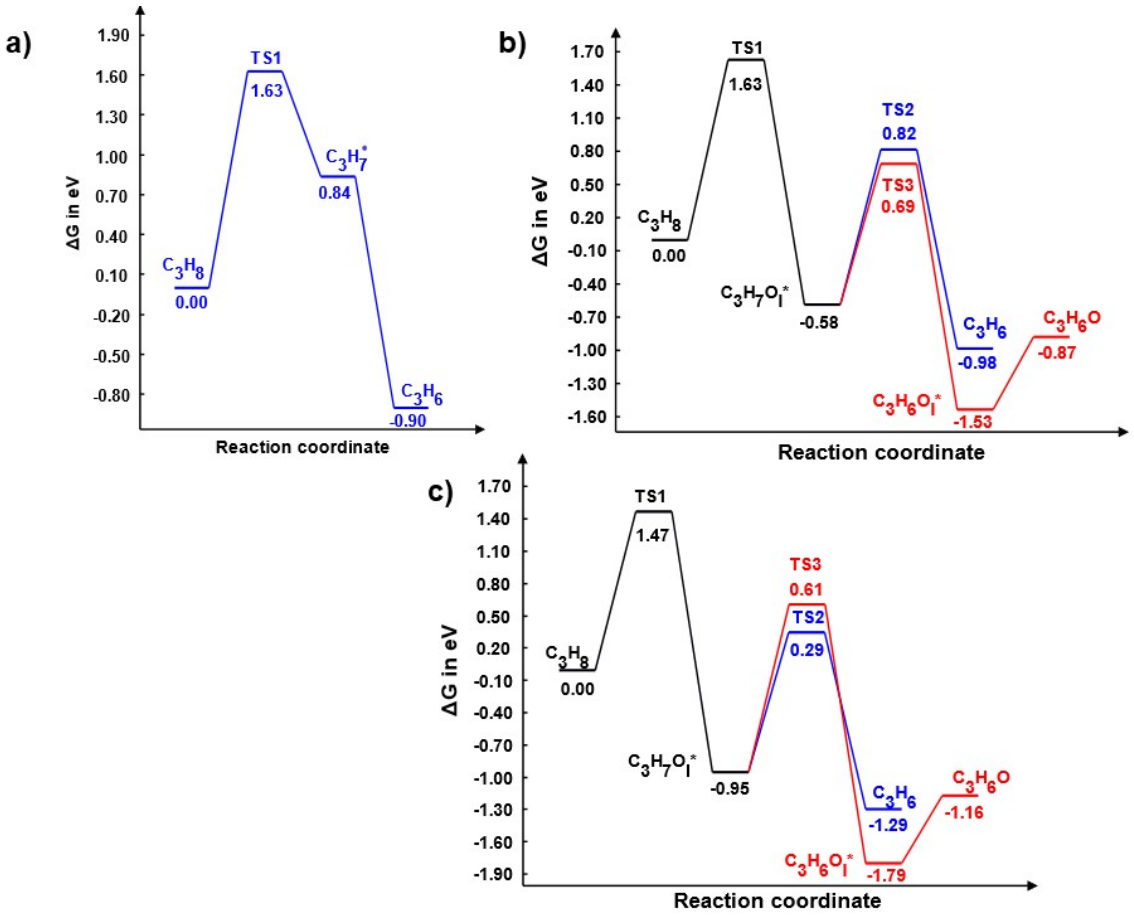

Figure S13. Gibbs free energy diagrams for a) S1-O_{bridge}, b) S1-S2-O_{bridge} and c) S2-S3-S7/S4 pathways over VO_2/CeO_2 (110) surface at T = 773 K. The corresponding potential energy diagrams to the above networks (a, b, and c in order) are shown in Figures 3 (red path), 4a, and 5a of the main manuscript. On comparison with the PESs, the energy and product formation trends were found to be qualitatively similar.

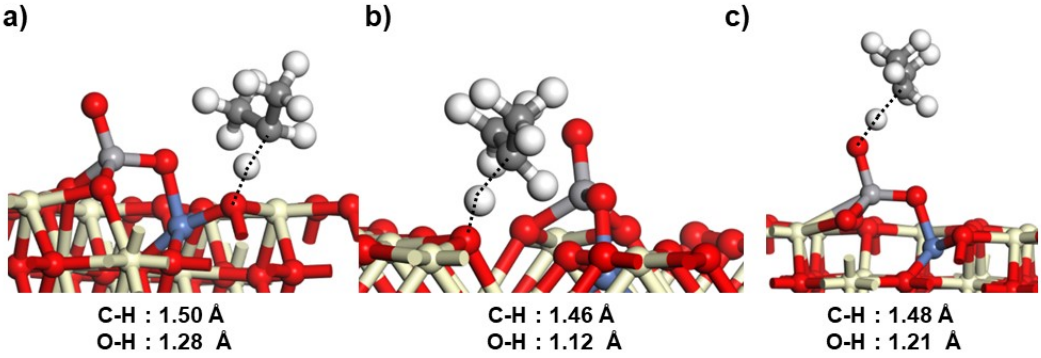

Figure S14. Structures and the activated bond lengths of the transition states in propane ODH mechanisms (isopropyl radical mediated) over $VO_2/Ce_{0.83}Ni_{0.17}O_2(110)$ surface, as shown in a) S1-O_{bridge} path, b) S4-O_{bridge} path and c) $O_{vanadyl}$-O_{bridge} path in Figure 6 of the manuscript. Here, the cream, red, light grey, blue, white and dark grey atoms denote Ce, O, V, Ni, H and C atoms, respectively.

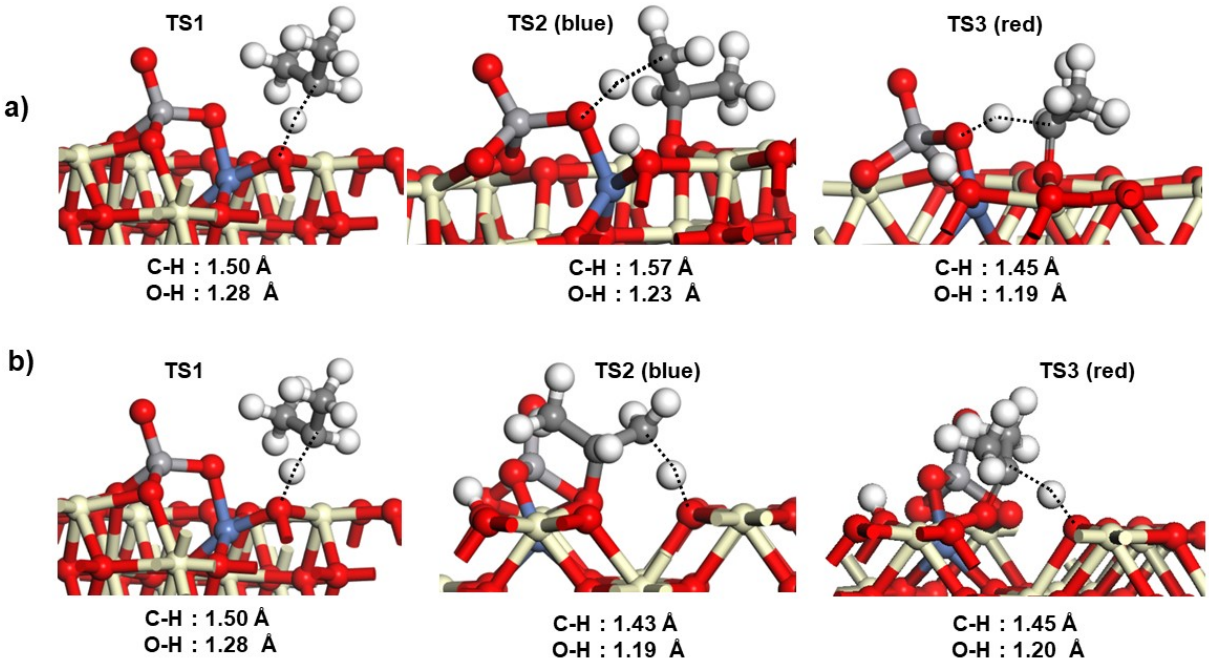

Figure S15. Structures and the activated bond lengths of the transition states in propane ODH mechanisms (isopropoxide mediated) over $VO_2/Ce_{0.83}Ni_{0.17}O_2(110)$ surface, as shown in a) S1-S2-O_{bridge} path, b) S1-S2-S3 path in Figure 7 of the manuscript. Here, the cream, red, light grey, blue, white and dark grey atoms denote Ce, O, V, Ni, H and C atoms, respectively.

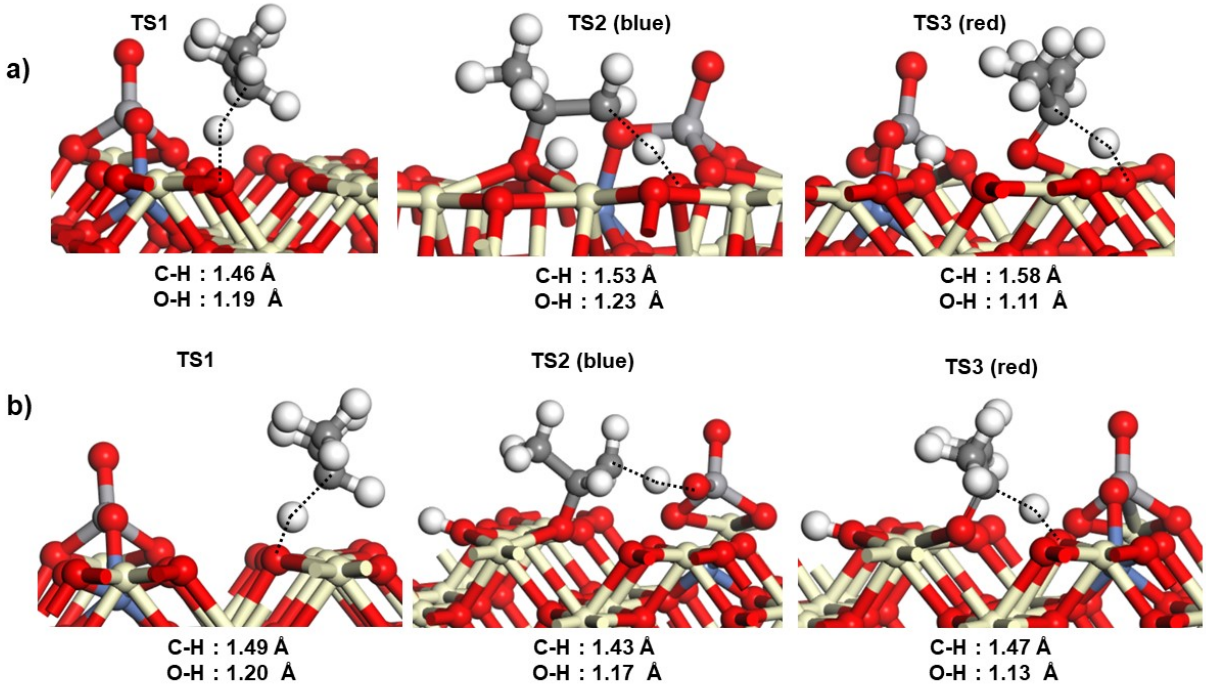

Figure S16. Structures and the activated bond lengths of the transition states in propane ODH mechanisms (isopropoxide mediated) over $VO_2/Ce_{0.83}Ni_{0.17}O_2(110)$ surface, as shown in a) S2-S3-S7/S4 path, b) S3-S4-O_{bridge}/S1 path in Figure 8 of the manuscript. Here, the cream, red, light grey, blue, white, and dark grey atoms denote Ce, O, V, Ni, H and C atoms, respectively.

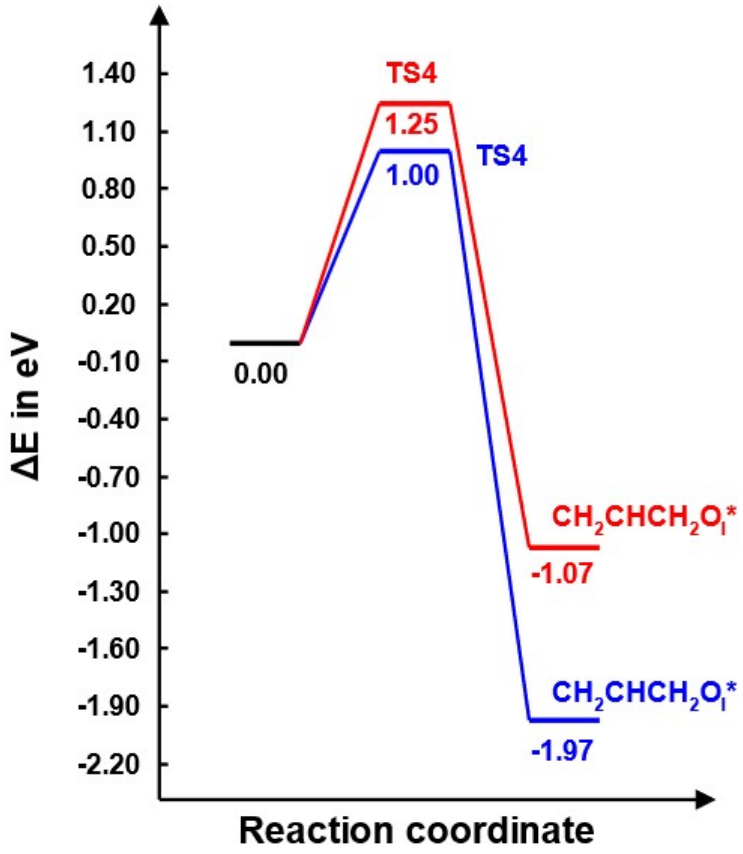

Figure S17. Comparison of the energy profiles for propene C-H activation steps over site S3, denoting the onset of sequential oxidation route for propane oxidation via propene formation over $VO_2/Ce_{0.83}Ni_{0.17}O_2(110)$ (red path) and $VO_2/CeO_2(110)$ (blue path) surfaces. Here, site S3 was chosen for the purpose of comparison as it was shown to be one of the most favorable sites for propene activation in Figure S12. (Refer to Figure 1 of the main manuscript for the oxygen site numbering convention)

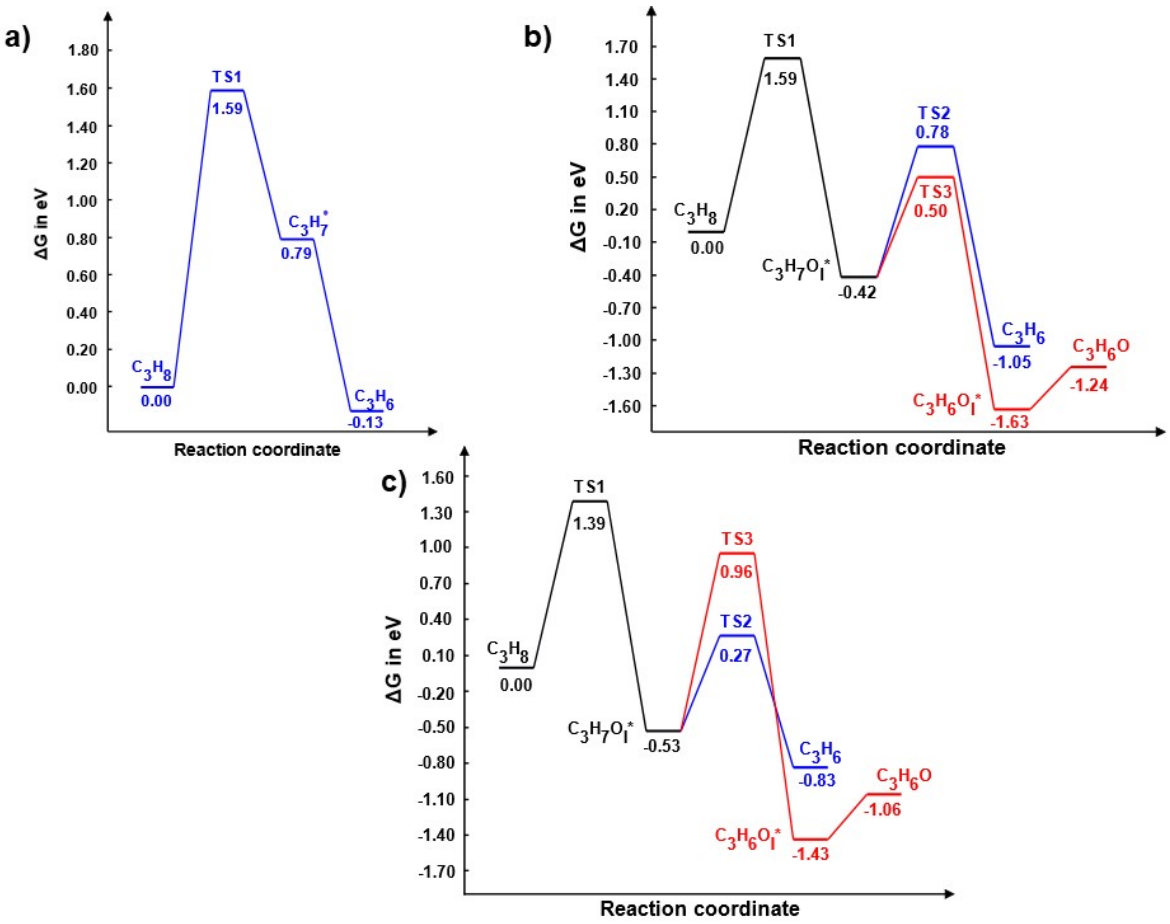

Figure S18. Gibbs free energy diagrams for a) S1-O_{bridge}, b) S1-S2-O_{bridge} and c) S2-S3-S7/S4 pathways over $VO_2/Ce_{0.83}Ni_{0.17}O_2$ (110) surface at T = 773 K. The corresponding potential energy diagrams to the above networks (a, b, and c in order) are shown in Figures 6 (red path), 7a, and 8a of the main manuscript. On comparison with the PESs, the energy and product formation trends were found to be qualitatively similar.

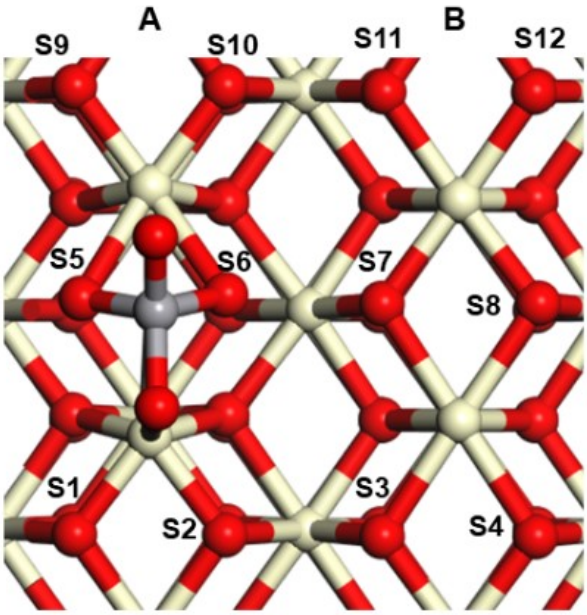

Figure S19. Representative catalyst model for 0.17 ML $VO_2/CeO_2(110)$

Table S6. Heuristic prediction of active oxygen combinations and their % contributions favoring propene and acetone formation over $VO_2/CeO_2(110)$ and $VO_2/Ce_{0.83}Ni_{0.17}O_2(110)$ surfaces, at 0.17 ML VO_2 coverages. The cells with green and red shading indicate dominant and submissive active site combinations respectively, in a parallel set of reaction pathways. The alphabets A and B inside the brackets denote the rows A and B as defined in Figure S19. The isopropyl radical-mediated mechanisms were not applicable for acetone formation and hence these are denoted with "–". Here, the mechanisms denoted by $ were studied in this work, while the rest of them were hypothesized based on the observations made in this work.

Pathway type	Propene	Acetone
C_3H_7• mediated	S1-O_{bridge} (A)$^{\$}$	-
	S4- O_{bridge} (A)$^{\$}$	-
	$O_{vanadyl}$ - O_{bridge} (A)$^{\$}$	-
	S2- O_{bridge} (A) $^{\$}$	-
$C_3H_7O_l$* mediated	S1-S2- O_{bridge} $^{\$}$	S1-S2- O_{bridge} $^{\$}$
	S1-S2-S10	S1-S2-S3 $^{\$}$
	S2-S3-S7 $^{\$}$	S2-S3-S4 $^{\$}$
	S2-S3-S11	
	S3-S2- O_{bridge}	S3-S2- O_{bridge}
	S3-S4-S8	S3-S4-S1 $^{\$}$

	S3-S4-S12	
	S4-S1- O_{bridge}	S4-S1- O_{bridge} $
	S4-S1-S9	S4-S1-S2
	S7-S8-S12	S7-S8-S5
	S7-S8-S4	
	S9-S10-S2	S9-S10-S11
	S10-S11-S3	S10-S11-S12
	S10-S11-S7	
	S11-S12-S4	S11-S12-S9
	S11-S12-S8	
	S12-S9-S1	S12-S9-S10
% Contribution	**71.43**	**43.75**

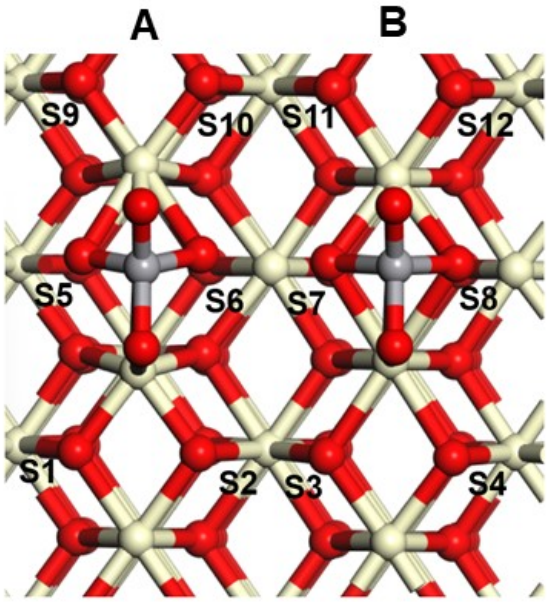

Figure S20. Representative catalyst model for 0.33 ML $VO_2/CeO_2(110)$

Table S7. Heuristic prediction of active oxygen combinations and their % contributions favoring propene and acetone formation over $VO_2/CeO_2(110)$ and $VO_2/Ce_{0.83}Ni_{0.17}O_2(110)$ surfaces, at 0.17 ML VO_2 coverages. The cells with green and red shading indicate dominant and submissive active site combinations respectively, in a parallel set of reaction pathways. The alphabets A and B inside the brackets denote the rows A and B as defined in Figure S20. The isopropyl radical mediated mechanisms were not applicable for acetone formation and hence these are denoted with "–". Here, all the mechanisms were hypothesized based on the observations made in this work. Notations of the form (x&y) denote sites present in rows 'x' and 'y' respectively (where (x,y) $\in$ (A, B) in Figure S17).

Pathway type	Propene	Acetone
$C_3H_7^\bullet$ mediated	S1-O_{bridge} (A)	-
	$O_{vanadyl}$ - O_{bridge} (A)	-
	S4- O_{bridge} (A)	-
	$O_{vanadyl}$ - O_{bridge} (B)	-
	S2- O_{bridge} (A)	-
	S2- O_{bridge} (B)	-
	S3- O_{bridge} (B)	-
	S4- O_{bridge} (B)	-
	$O_{vanadyl}$ - $O_{vanadyl}$ (A&B)	-
$C_3H_7O_l$* mediated	S1-S2- O_{bridge}	S1-S2- O_{bridge}
	S1-S2-S10	S1-S2-S3

	S2-S3- O_{bridge}	S2-S3- O_{bridge}
	S2-S3-S11	S2-S3-S4
	S3-S4- O_{bridge}	S3-S4- O_{bridge}
	S3-S4-S8	S3-S4-S1
	S4-S1- O_{bridge}	S4-S1- O_{bridge}
	S4-S1-S9	S4-S1-S2
	S9-S10-S2	S9-S10-S11
	S10-S11-S3	S10-S11-S12
	S11-S12-S4	S11-S12-S9
	S12-S9-S1	S12-S9-S10
% Contribution	**80.95**	**38.10**

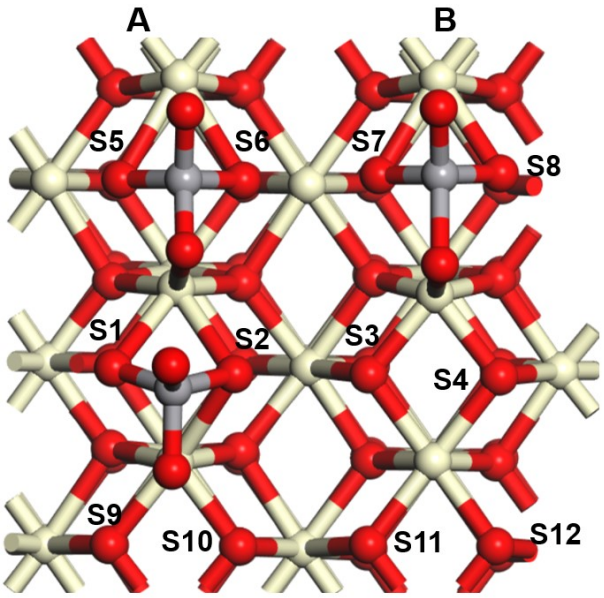

Figure S21. Representative catalyst model for 0.50 ML $VO_2/CeO_2(110)$

Table S8. Heuristic prediction of active oxygen combinations and their % contributions favoring propene and acetone formation over $VO_2/CeO_2(110)$ and $VO_2/Ce_{0.83}Ni_{0.17}O_2(110)$ surfaces, at 0.50 ML VO_2 coverages. The cells with green and red shading indicate dominant and submissive active site combinations respectively, in a parallel set of reaction pathways. The alphabets A and B inside the brackets denote the rows A and B as defined in Figure S21. The isopropyl radical mediated mechanisms were not applicable for acetone formation and hence these are denoted with "–". Here, all the mechanisms were hypothesized based on the observations made in this work. Notations of the form (x&y) denote sites present in rows 'x' and 'y' respectively (where (x,y) $\in$ (A, B) in Figure S18).

Pathway type	Propene	Acetone
$C_3H_7^\bullet$ mediated	S4-O_{bridge} (B)	-
	$O_{vanadyl}$ - O_{bridge} (B)	-
	S3- O_{bridge} (B)	-
	S4- O_{bridge} (A)	-
	$O_{vanadyl}$ - O_{bridge} (A)	-
	S9- O_{bridge} (A)	-
	S10-O_{bridge} (A)	-
	S12- O_{bridge} (A)	-
	$O_{vanadyl}$ - O_{bridge} (A)	-
	$O_{vanadyl}$ - O_{bridge} (A&B)	-
	$O_{vanadyl}$ -O_{bridge} (A&A)	-

	$O_{vanadyl}$ - $O_{vanadyl}$ (A&B)	-
	$O_{vanadyl}$ - $O_{vanadyl}$ (A)	-
$C_3H_7O_l$* mediated	S3-S4- O_{bridge}	S3-S4- O_{bridge}
	S3-S4-S12	S3-S4-S1
	S9-S10- O_{bridge}	S9-S10- O_{bridge}
	-	S9-S10-S11
	S10-S11-S3	S10-S11-S12
	S11-S10- O_{bridge}	S11-S10- O_{bridge}
	S11-S12-S4	S11-S12-S9
	S12-S9- O_{bridge}	S12-S9- O_{bridge}
% Contribution	**90.48**	**28.57**

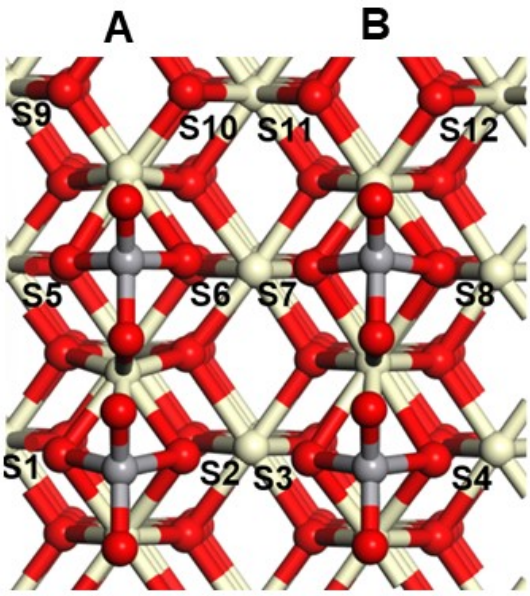

Figure S22. Representative catalyst model for 0.67 ML $VO_2/CeO_2(110)$

Table S9. Heuristic prediction of active oxygen combinations and their % contributions favoring propene and acetone formation over $VO_2/CeO_2(110)$ and $VO_2/Ce_{0.83}Ni_{0.17}O_2(110)$ surfaces, at 0.50 ML VO_2 coverages. The cells with green and red shading indicate dominant and submissive active site combinations respectively, in a parallel set of reaction pathways. The alphabets A and B inside the brackets denote the rows A and B as defined in Figure S22. The isopropyl radical mediated mechanisms were not applicable for acetone formation and hence these are denoted with "–". Here, all the mechanisms were hypothesized based on the observations made in this work. Notations of the form (x&y) denote sites present in rows 'x' and 'y' respectively (where (x,y) $\in$ (A, B) in Figure S19).

Pathway type	Propene	Acetone
$C_3H_7^\bullet$ mediated	S11-O_{bridge} (B)	-
	$O_{vanadyl}$ - O_{bridge} (B)	-
	S12- O_{bridge} (B)	-
	$O_{vanadyl}$ - O_{bridge} (B)	-
	$O_{vanadyl}$ - O_{bridge} (B&B)	-
	S9- O_{bridge} (A)	-
	S10- O_{bridge} (A)	-
	S12- O_{bridge} (A)	-
	$O_{vanadyl}$ - O_{bridge} (A)	-
	$O_{vanadyl}$ - O_{bridge} (A)	-
	$O_{vanadyl}$ - O_{bridge} (A&A)	-

	$O_{vanadyl}$ - O_{bridge} (A&B)	-
	$O_{vanadyl}$ - O_{bridge} (B&A)	-
	$O_{vanadyl}$ - $O_{vanadyl}$ (A&A)	-
	$O_{vanadyl}$ - $O_{vanadyl}$ (A&B)	-
	$O_{vanadyl}$ - $O_{vanadyl}$ (A&B)	-
	$O_{vanadyl}$ - $O_{vanadyl}$ (B&B)	-
$C_3H_7O_l$* mediated	-	S9-S10-S11
	S9-S10- O_{bridge}	S9-S10- O_{bridge}
	S10-S11- O_{bridge}	S10-S11- O_{bridge}
	S12-S9- O_{bridge}	S10-S11-S12
	S11-S12- O_{bridge}	S11-S12- O_{bridge}
	-	S11-S12-S9
	S12-S9- O_{bridge}	S12-S9- O_{bridge}
% Contribution	**91.30**	**25.00**

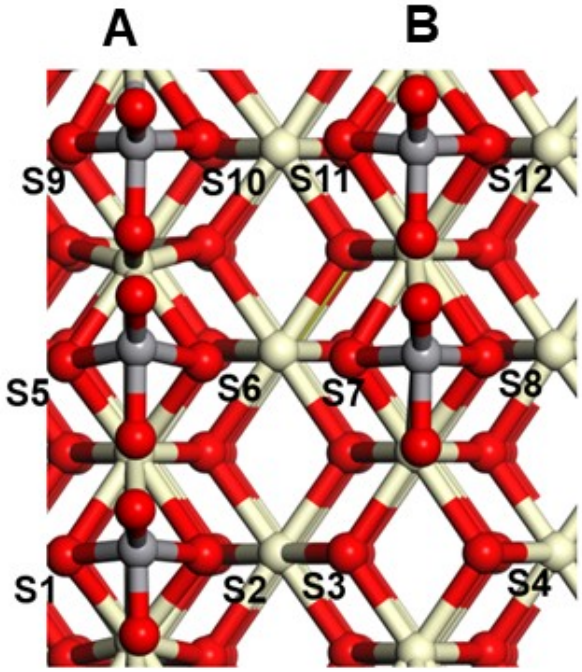

Figure S23. Representative catalyst model for 0.83 ML $VO_2/CeO_2(110)$

Table S10. Heuristic prediction of active oxygen combinations and their % contributions favoring propene and acetone formation over $VO_2/CeO_2(110)$ and $VO_2/Ce_{0.83}Ni_{0.17}O_2(110)$ surfaces, at 0.50 ML VO_2 coverages. The cells with green and red shading indicate dominant and submissive active site combinations respectively, in a parallel set of reaction pathways. The alphabets A and B inside the brackets denote the rows A and B as defined in Figure S23. The isopropyl radical mediated mechanisms were not applicable for acetone formation and hence these are denoted with "–". Here, all the mechanisms were hypothesized based on the observations made in this work. Notations of the form (x&y) denote sites present in rows 'x' and 'y' respectively (where (x,y) $\in$ (A, B) in Figure S20).

Pathway type	Propene	Acetone
$C_3H_7^\bullet$ mediated	S3-O_{bridge} (B)	-
	$O_{vanadyl}$ - O_{bridge} (B)	-
	S4- O_{bridge} (B)	-
	S4- O_{bridge} (A)	-
	$O_{vanadyl}$ - O_{bridge} (B)	-
	$O_{vanadyl}$ - O_{bridge} (A)	-
	$O_{vanadyl}$ - O_{bridge} (A)	-
	$O_{vanadyl}$ - O_{bridge} (A)	-
	$O_{vanadyl}$ - O_{bridge} (A&A)	-

	$O_{vanadyl}$ - O_{bridge} (A&A)	-
	$O_{vanadyl}$ - O_{bridge} (A&A)	-
	$O_{vanadyl}$ - O_{bridge} (B&B)	-
	$O_{vanadyl}$ - O_{bridge} (A&B)	-
	$O_{vanadyl}$ - O_{bridge} (A&B)	-
	$O_{vanadyl}$ - O_{bridge} (A&B)	-
	$O_{vanadyl}$ - $O_{vanadyl}$ (A&A)	-
	$O_{vanadyl}$ - $O_{vanadyl}$ (A&A)	-
	$O_{vanadyl}$ - $O_{vanadyl}$ (A&A)	-
	$O_{vanadyl}$ - $O_{vanadyl}$ (A&B)	-
	$O_{vanadyl}$ - $O_{vanadyl}$ (A&B)	-
$C_3H_7O_l$* mediated	S3-S4- O_{bridge}	S3-S4- O_{bridge}
% Contribution	**100**	**4.76**

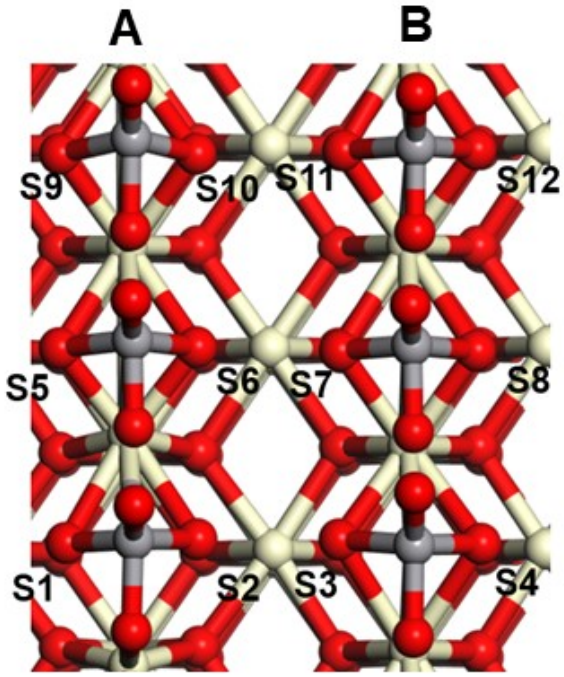

Figure S24. Representative catalyst model for 1.00 ML $VO_2/CeO_2(110)$

Table S11. Heuristic prediction of active oxygen combinations and their % contributions favoring propene and acetone formation over $VO_2/CeO_2(110)$ and $VO_2/Ce_{0.83}Ni_{0.17}O_2(110)$ surfaces, at 0.50 ML VO_2 coverages. The cells with green and red shading indicate dominant and submissive active site combinations respectively, in a parallel set of reaction pathways. The alphabets A and B inside the brackets denote the rows A and B as defined in Figure S24. The isopropyl radical mediated mechanisms were not applicable for acetone formation and hence these are denoted with "–". Here, all the mechanisms were hypothesized based on the observations made in this work. Notations of the form (x&y) denote sites present in rows 'x' and 'y' respectively (where (x,y) $\in$ (A, B) in Figure S21).

Pathway type	Propene	Acetone
$C_3H_7^\bullet$ mediated	$O_{vanadyl}$ -O_{bridge} (A)	-
	$O_{vanadyl}$ -O_{bridge} (A)	-
	$O_{vanadyl}$ -O_{bridge} (A)	-
	$O_{vanadyl}$ -O_{bridge} (B)	-
	$O_{vanadyl}$ -O_{bridge} (B)	-
	$O_{vanadyl}$ -O_{bridge} (B)	-
	$O_{vanadyl}$ -O_{bridge} (A&A)	-
	$O_{vanadyl}$ -O_{bridge} (A&A)	-
	$O_{vanadyl}$ -O_{bridge} (A&A)	-

	$O_{vanadyl}$ -O_{bridge} (A&B)	-
	$O_{vanadyl}$ -O_{bridge} (A&B)	-
	$O_{vanadyl}$ -O_{bridge} (A&B)	-
	$O_{vanadyl}$ -O_{bridge} (B&B)	-
	$O_{vanadyl}$ -O_{bridge} (B&B)	-
	$O_{vanadyl}$ -O_{bridge} (B&B)	-
	$O_{vanadyl}$ -O_{bridge} (B&A)	-
	$O_{vanadyl}$ -O_{bridge} (B&A)	-
	$O_{vanadyl}$ -O_{bridge} (B&A)	-
	$O_{vanadyl}$ -$O_{vanadyl}$ (A&A)	-
	$O_{vanadyl}$ -$O_{vanadyl}$ (A&A)	-
	$O_{vanadyl}$ -$O_{vanadyl}$ (A&A)	-
	$O_{vanadyl}$ -$O_{vanadyl}$ (A&B)	-
	$O_{vanadyl}$ -$O_{vanadyl}$ (A&B)	-
	$O_{vanadyl}$ -$O_{vanadyl}$ (A&B)	-
	$O_{vanadyl}$ -$O_{vanadyl}$ (B&B)	-
	$O_{vanadyl}$ -$O_{vanadyl}$ (B&B)	-
	$O_{vanadyl}$ -$O_{vanadyl}$ (B&B)	-
% Contribution	**100.00**	**0.00**

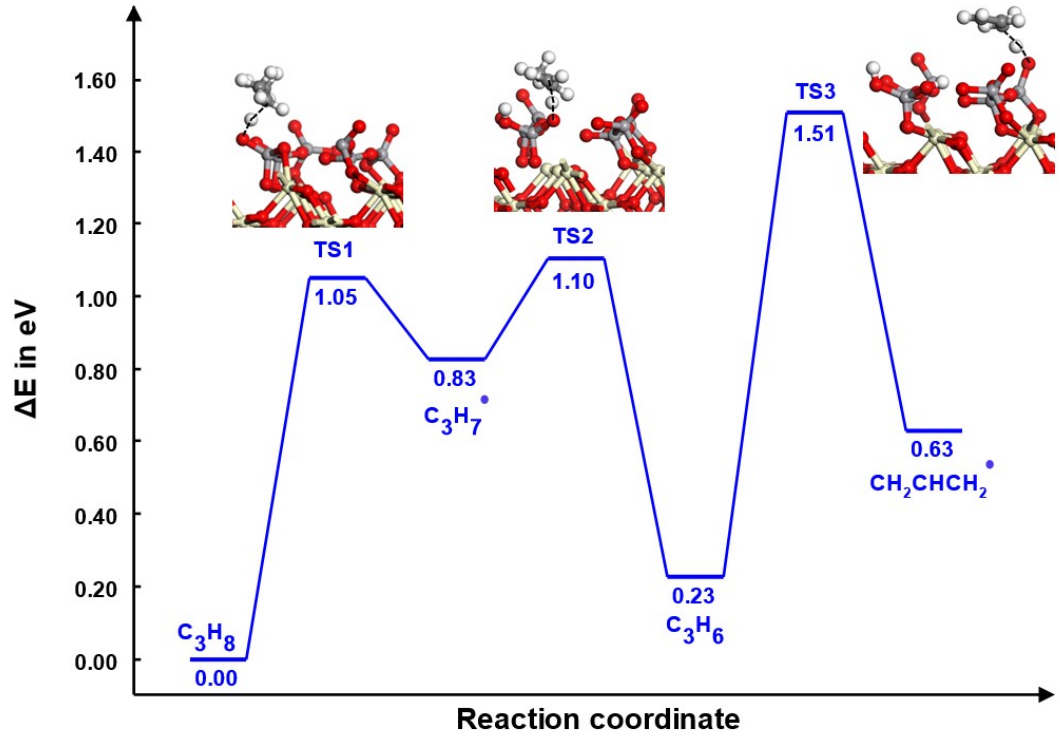

Figure S25. Energy profile for first three C-H activations of Propane, denoting the Propane ODH (isopropyl radical mediated) and onset of sequential oxidation (propene C-H activation) mechanism over 1ML $VO_2/CeO_2(110)$ surface. The direct oxidation of propane via the formation of undesired C_3H_6O was not feasible due to inaccessibility of ceria surface oxygens to propane and its constituent intermediates.

References

(1) Varghese, J. J.; Mushrif, S. H. Insights into the C-H Bond Activation on NiO Surfaces: The Role of Nickel and Oxygen Vacancies and of Low Valent Dopants on the Reactivity and Energetics. *Journal of Physical Chemistry C* **2017**, *121* (33), 17969–17981. https://doi.org/10.1021/acs.jpcc.7b05226.

(2) Rohrbach, G.; Hafner, J.; Kresse, G. Molecular Adsorption on the Surface of Strongly Correlated Transition-Metal Oxides: A Case Study for CO/NiO(100). *Phys Rev B Condens Matter Mater Phys* **2004**, *69* (7).

(3) Wu, X.; Yu, X.; Huang, Z.; Shen, H.; Jing, G. MnOx-Decorated VOx/CeO2 Catalysts with Preferentially Exposed {110} Facets for Selective Catalytic Reduction of NOx by NH3. *Appl Catal B* **2020**, *268*, 118419.